Efficiency of a gyroscopic device for conversion of mechanical wave energy to electrical energy

M. Carlsen[*], R. Darula[†], J. Gravesen[*], P.G. Hjorth[*],
H.B. Jørgensen[‡], D.M. Nguyen[*], P.N. Nielsen[*],
J. Olsen[§], H.G. Petersen[‡], P. Røgen[*], M. Ögren[*]

November 9, 2011

[*]Technical University of Denmark
[†]Aalborg University
[‡]University of Southern Denmark
[§]Joltech

Abstract

We consider a recently proposed gyroscopic device for conversion of mechanical ocean wave energy to electrical energy. Two models of the device derived from standard engineering mechanics from the literature are analysed, and a model is derived from analytical mechanics considerations. From these models, estimates of the power production, efficiency, forces and moments are made. We find that it is possible to extract a significant amount of energy from an ocean wave using the described device. Further studies are required for a full treatment of the device.

Contents

1 Introduction

Recently, Joltech has proposed a gyroscopic device for conversion of mechanical energy in ocean surface waves to electrical energy [Olsen, 2011b]. This gyroscopic device is the focus of the current project report. The objectives are first to establish mathematical models for the gyroscopic device, and second, from these models, to estimate its power production, its optimal efficiency and the forces and torques working on it under operating conditions.

The report constitutes the written answer to the question posed by Joltech at the 83rd European Study Group with Industry (ESGI 83), taking place on August 15–19, 2011 in Sønderborg, Denmark. During the 5 days ESGI 83 event, a group consisting of the authors of this report worked on the project together. This report documents the work carried out by the group during this week.

The outline of the report is as follows. First, the basic principles of the gyroscopic device are described in section 2, followed by a brief introduction to ocean surface waves in section 3. Then, in section 4, two models of the motion of the device in the literature are reviewed and extended, and the power output, forces and torques are estimated from this, and bifurcation and stability analysis are presented. In section 5, a mathematical model of the device is derived from an analytical mechanics approach and the efficiency, forces and torques are estimated from this. Finally, we conclude and outline future work in section 6.

2 Description of the Gyroscopic Device

The gyroscopic device analyzed consists of three major parts (Fig. 1):

- *Arm*: fixed at one end and free at the other, used to constrain the motion of the ball. The arm has two degrees of freedom, i.e. it cannot rotate around its own axis, however it can move the attached ball around on a spherical (or hemi-spherical) surface path.
- *Ball*: fixed to the free end of the arm. The ball encapsulates the gyroscopic device and serves as a buoy, i.e. floats on the water.
- *Gyroscopic device*: inside the ball. It consists of:
  - *A flywheel*: used to 'store' energy. It is a disc (or another axisymmetric body) freely rotating around the shaft.
  - *Outer ring*: a circular path which allows the shaft of the flywheel to rotate freely in a circle.

The operation principle of the device is similar to Archie Mischler's invention, a "hand-held gyroscope" [Mischler, 1973]. Gulick [Gulick and O'Reilly, 2000] cites the part of the patent describing how it works: '*new gyroscopic device in which the rotor cannot only rotate about its spin axis but can also rotate about a second axis at right angles to the spin axis, and in which the rotor can be made to increase in speed by applying a torque about a third axis*'. The gyroscopic device is sold as a

"wrist exerciser" under the names Dynabee, Powerball, Roller Ball or Dyna-Flex. Several articles analyzing the dynamics of this hand held gyroscope have been pulished, e.g. [Gulick and O'Reilly, 2000] and [Heyda, 2002]. The human motion while turning the toy is presented in [Gams et al., 2007]. The gyroscopic device analysed in this report is of course on a much larger scale than this hand-held model.

2.1 Motion of the Ball

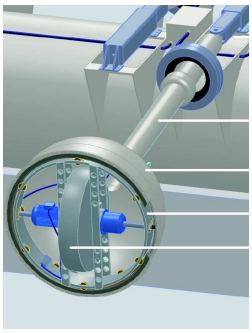

Figure 1: Drawing of the device [Olsen, 2011a].

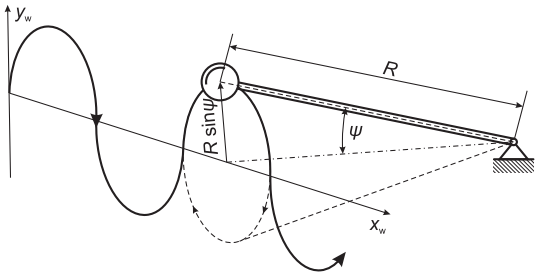

Figure 2: Schematics of system exposed to incoming wave.

The overall motion of the device on the water is presented in Fig. 2. We start by assuming that the ball attached to the arm simply just follows the motion of the incoming wave. Assuming sufficiently deep water, the particle exposed to water surface gravity wave will follow a circular path [Holthuijsen, 2007], as shown in Fig 9. Then the motion of the ball can be expressed using e.g. Cartesian coordinates as:

$$x_w = A\sin(\omega t) = R\sin(\psi)\sin\left(\frac{2\pi}{T}t\right), \tag{1a}$$

$$y_w = A\cos(\omega t) = R\sin(\psi)\cos\left(\frac{2\pi}{T}t\right), \tag{1b}$$

where $A = R\sin(\psi)$ is the amplitude of the wave. The angular velocity can be expressed as $\omega = 2\pi/T$ (in rad/s), where T (in s) is the period of the wave motion.

2.2 Motion of the Gyroscopic Device

The motion of the gyroscopic device inside the ball is sketched in Fig. 4. All in all, we can distinguish three types of motion:

- *Flywheel rotation* ($\dot{\gamma}$): rotation of the flywheel around its axis of rotation.
- *Axle rotation* ($\dot{\alpha}$): rotation of the flywheel's axle inside the groove of the outer ring.
- *Ball rotation* ($\dot{\delta}$): rotation of the ball fixed to arm.

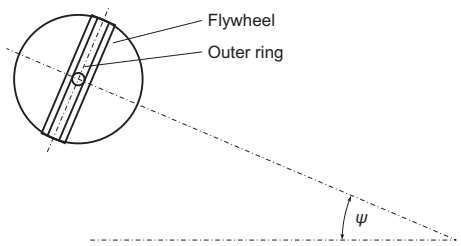

Figure 3: Schematics of device with definition of precession angle ψ.

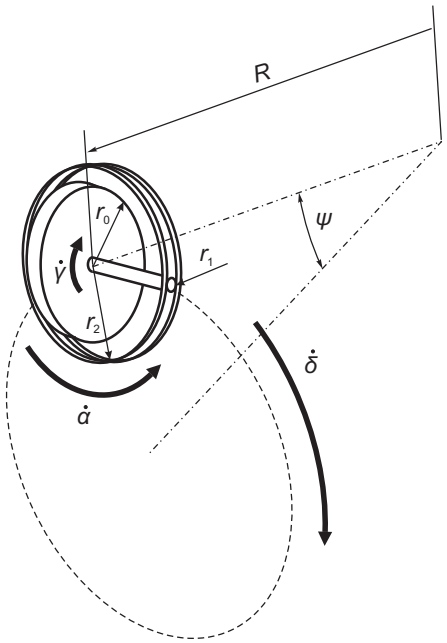

Figure 4: Schematics of the gyroscopic device with motion definitions.

The outer ring undergoes a precessional motion with angle ψ, as shown in Fig. 3. When the flywheel is at rest, nothing happens and even exposing the ball to circular motion (Fig. 2), the flywheel's axis will just follow the motion of the wave. As soon as the flywheel is set into rotational motion ($\dot{\gamma} \neq 0$), and exposed to precessional motion ($\dot{\delta} \neq 0$), the axle starts to move along the outer ring. When the motion of the precession is synchronized with the flywheel rotational speed ($\dot{\gamma} = -r_2/r_1\dot{\psi}$), the rotor keeps the steady-state rotation. In the report, when the steady-state operation is assumed, the shaft of the flywheel rolls without any slip on the outer ring, as indicated in Fig. 5.

Parameters used in the further analysis are summarised in Tab. 1.

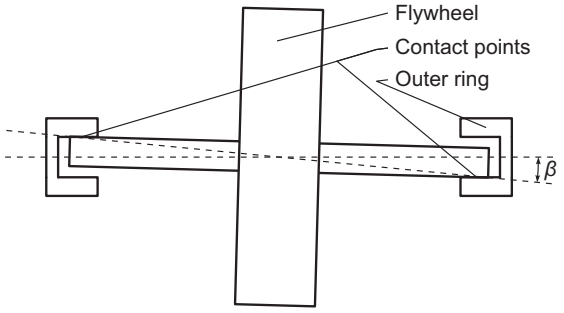

Figure 5: Schematics of rolling contact after [Gulick and O'Reilly, 2000]

Parameter	Description
R	Length of the arm
r_0	Radius of flywheel
r_1	Radius of the flywheel's shaft
r_2	Radius of the outer ring
ψ	Precession angle
$\dot{\gamma}$	Flywheel angular velocity
$\dot{\alpha}$	Flywheel axle angular velocity
$\dot{\delta}$	Ball angular velocity

Table 1: Description of parameters.

3 Ocean Surface Waves

In describing the behavior of water, we can use an idealized concept and treated water as an incompressible inviscous fluid [Holthuijsen, 2007], a medium in which the wave ideally propagates without any change of amplitude, frequency or phase.

3.1 Motion of Fluid Particles

Ocean waves, also known as "*wind generated surface gravity waves*" [Holthuijsen, 2007], are created at the water free surface, i.e. at the interface between water and air. According to [Bhattacharyya, 1978], a wave in the ocean can be defined as a "*transverse disturbance, since the motion of particles is apparently in one direction (i.e. up and down) and the direction of propagation of the disturbance is at a right angle to the direction of motion*".

Holthuijsen [Holthuijsen, 2007] introduces two principal parameters of the wave (Fig. 6):

- *Wave height* (H): The distance between the highest and lowest surface elevation in the wave.

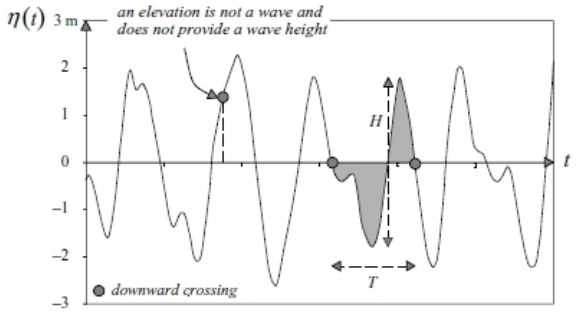

Figure 6: Visualisation of the height and period of a wave [Holthuijsen, 2007].

- *Wave period* (T): The time interval between two adjacent zero down-crossings.

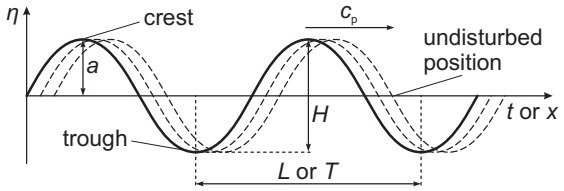

Figure 7: Sine wave approximation of the wave after [Holthuijsen, 2007] and [Bhattacharyya, 1978].

Bhattacharyya [Bhattacharyya, 1978] idealizes the water surface waves in ocean assuming sinusoidal waves, characterized by (Fig. 7):

- *Wave crest/trough*: a point with highest/lowest elevation.
- *Amplitude of wave* (a): a vertical distance between the wave crest and undisturbed water surface (or half of wave height (H), i.e. the vertical distance between crest and trough).
- *Wave length* (L): a distance from a crest to a next one.
- *Phase velocity* (c_p): a distance at which e.g. crest travel in one second.
- *Characteristic frequency* (f): number of crests/troughs passing given point in one second (it is valid that $f = c_p/L$).

Based on derivations, summarized e.g. in [Holthuijsen, 2007], depending on the depth of water, we can conclude that:

- In deep water, the circular motion of the particles is observed (Fig. 8 - left figure).
- The more shallow the water is, the more elliptic the particle orbits become (Fig. 8 - mid and right figure).

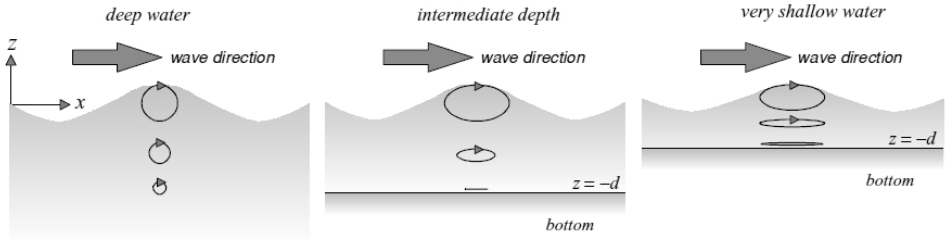

Figure 8: Depth of water and motion of the particle [Holthuijsen, 2007]

Therefore, under the assumption of sufficiently deep water, the motion of the water particle, and hence a body following directly the surface water particles, is circular (Fig. 9), and the wave can be idealized as a sine wave. The motion is then described by equations (1).

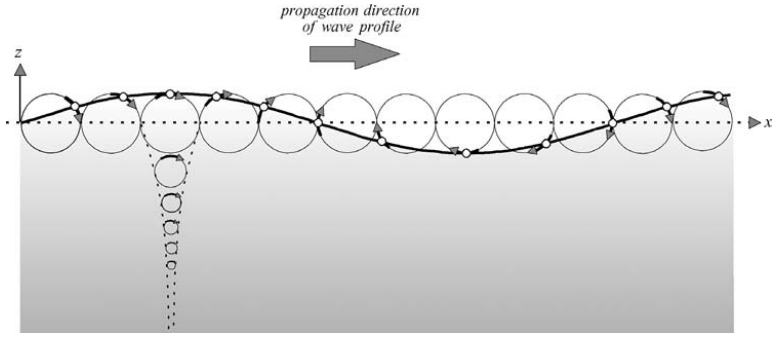

Figure 9: Wave profile of water gravity waves [Holthuijsen, 2007].

3.2 Energy of Waves

The wave in the fluid propagates due to *inertia of the fluid* and *gravity*, which tends to maintain the fluid in a horizontal plane [Bhattacharyya, 1978]. The *kinetic energy* of the system is due to the orbital motion of water particles. The kinetic energy per unit width of the wave:

$$E_k = \frac{1}{4}\rho g a^2 L \tag{2}$$

with fluid density ρ, acceleration due to gravity g, wave amplitude a and wave length L. The *potential energy* is due to elevation change of the water level. The potential energy per unit width of the wave:

$$E_p = \frac{1}{4}\rho g a^2 L \tag{3}$$

The *total energy*, as discussed in [Bhattacharyya, 1978], is a sum of the two ones:

$$E = E_k + E_p = \frac{1}{2}\rho g a^2 L \tag{4}$$

A similar expression of total energy is presented also in [Falnes, 2002].

3.3 Body-water Interaction

As discussed e.g. in [Ogihara, 1980], a spherical object, like the buoy in the present report, submerged partially in the water and fixed with e.g. flexible string, will be exposed to water-structure interaction, i.e. so-called Morison's expression of the forces need to be taken into account [Fish et al., 1980]:

$$dF = \frac{1}{2}C_D \rho D U^2 ds + C_m \rho A U ds \tag{5}$$

which is the sum of drag and fluid inertia force. Parameters C_D and C_m are drag and inertia coefficients and dependend on fluid and shape of the structure, ρ is density of water, ds length element, D is body dimension, A cross-sectional area and U water particle velocity.

Deeper discussion of parameters and some estimated coefficients of C_D and C_m are presented e.g. in [Fish et al., 1980]. Some utilization of Morison's equations to analyze numerically the oscillatory flows of cylindrical bodies (using so-called vortex method) can be found in [Smith and Stansby, 1991].

A discussion on water impacts, off-shore structures are exposed to as well, presents [Garrison, 1996]. The circular structural elements are analyzed and it is concluded that the Morison's equation is not applicable. Another energy methods are presented.

4 Two Models Treated in the Literature

In this section two models of the device from the literature are reviewed and extended. The power output, forces and torques are estimated, and bifurcation and stability analysis are presented.

4.1 Model 1

We consider firstly a model based on rigid-body dynamics with a fixed center of mass of the fly wheel. The model is derived in [Gulick and O'Reilly, 2000] and is illustrated in Fig. 10. Note that the center of mass of the fly wheel is fixed. It is therefore the arm and not the fly wheel that is in the water in this model.

The assumptions for this model are summarized below:

1. The precession rate, $\dot{\Psi}$, is the only external degree of freedom.
2. The floater is assumed to move on a circle with constant speed, cf. Sec. 2.1.

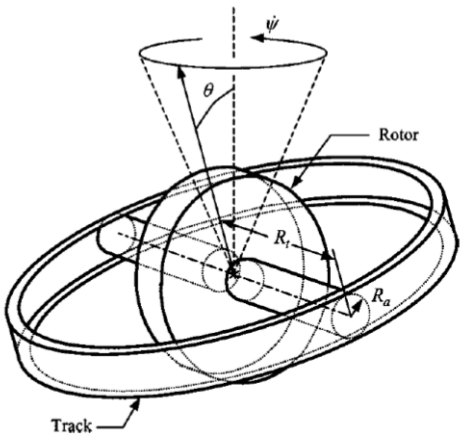

Figure 10: A model of a dynabee that precesses about a fixed angle (from [Gulick and O'Reilly, 2000]).

3. The rotation of the fly wheel about the second axis (along its track) is synchronized with the the frequency of the water waves.
4. The center of mass of the fly wheel is fixed in space.
5. The generator acts as a frictional force that slows down the rotor. This dissipative moment is assumed to be proportional to the frequency of the rotor.

The first condition holds if the arm follow a water wave with constant frequency. The second condition is more restrictive since the experiment has to be set up such that the amplitude of water (and the length of the arm) is constant which restrict the applications of this model. This might be the main difference between this model and a general approach where the nutation angle, θ, is not fixed. The third condition might be difficult to achieve since we have not fully investigated the effect of the transients. It is important to note that this problem should also be examined experimentally. When the coupling between the fly wheel and the water waves is synchronized then the relative phase angle, δ is constant. δ is the difference in phase between the instantanious phase of the rotor axle and the phase of the track corresponding to precessing a cup around its center of mass. Then δ would be the phase between the bottom of the cup and the axle so when synchronized the axle just follows the bottom of the cup with a constant phase difference. Synchronization also means that the precession rate of the flywheel in the water and the precession the flywheel along its track is equal which is a visible effect that could be measured in the laboratory. The fourth condition is not expected to be important whereas the last condition is a common model of a generator.

The model has the following input parameters:

- σ damping constant.

- R_t half the length of the flywheel axle.
- R_a radius of the flywheel axle.
- r radius of the flywheel.
- H water wave amplitude
- R length of the arm
- ρ density of the flywheel
- T period of the water waves
- $\theta = \arcsin(H/R)$ constant angle between the amplitude of the wave and the arm.

We shall define $\zeta = R_t/R_a$ as the ratio between the two radii.

4.1.1 Power Output

This model can be used to give a quick estimate of the power output for a choice of input parameters. In the following we derive a simple expression for the power as a function of the input parameters.

A flywheel operates like a gyroscope. A rotor that is in spin has an angular frequency, ω_1, and an angular momentum $\boldsymbol{J} = \boldsymbol{\omega}_1\lambda$. A moment

$$\boldsymbol{M} = \boldsymbol{R_t} \times \boldsymbol{F_N} = \frac{d\boldsymbol{J}}{dt} \tag{6}$$

or

$$d\boldsymbol{J} = \boldsymbol{M}dt \tag{7}$$

applied to the rotor is completely analogous to a force applied to a particle with a momentum. The rotational analogous to applying a drag force is a dissipative moment

$$\boldsymbol{M}_{r_d} = -\sigma\omega_1\boldsymbol{e}_1 \tag{8}$$

that decreases $|\boldsymbol{J}|$ where $\boldsymbol{e}_1||\boldsymbol{J}$ and the rotational analogous to a force applied orthogonal to a particle with a momentum is a moment that changes the direction of $\boldsymbol{J}$ but not its norm $|\boldsymbol{J}|$ which is the cause of the spin rotating about its second axis.

The power can be calculated when the system is synchronized. Then the power of the dissipative moment is

$$P_{\text{sync}} = \sigma\omega_1^2. \tag{9}$$

We would like calculate the optimal $P_{\max}$ which we define as the maximum value of σ that can be put on the rotor without destroying the stability of the system.

It is possible to show that

$$\omega_1 = \dot{\Psi}_0 \left\{\sin\delta\sin\theta - \zeta\right\}. \tag{10}$$

The unknown variable to calculate ω_1 is therefore δ since σ, ζ, Ψ and θ are known where δ is the relative phase (see Fig. 3 in [Gulick

and O'Reilly, 2000]). Assuming a constant track precession rate and synchronization then δ is given by the algebraic equation

$$b\cos\delta - c\sin\delta - d\sin 2\delta = 0 \tag{11}$$

This equation can further be approximated if we assume that

$$\frac{1}{\zeta^2} << \eta \tag{12}$$

(then $d \approx 0$ and $c\sin\delta << a$, see equation 24 and 27 in the article) and δ can then be found from

$$\cos\delta \approx \frac{\xi\sigma}{\lambda\dot{\Psi}_0\sin\theta}. \tag{13}$$

where λ is principal inertia of moment around the rotor's axis of symmetry given by

$$\lambda = \frac{1}{2}\rho h\pi r^4 \tag{14}$$

Note that for any solution δ_0, $-\delta_0$ is also a solution so there are 2 solutions for δ (see the discussion below about the stability of the solutions). The power for a given σ can be found by combining (10) and (13). We can set an upper limit on σ by noting that $\cos\delta \leq 1$:

$$\frac{\xi\sigma}{\lambda\dot{\Psi}_0\sin\theta} \leq 1. \tag{15}$$

σ obviously has an upper limit because of the high dissipative moment. The upper limit on σ is given by the equation above such that the maximum value of σ is:

$$\sigma = \frac{\lambda\dot{\phi_0}\sin\theta}{\xi} \tag{16}$$

It is important to note that σ should in practice be less than $\sigma_{\max}$ for the system to withstand perturbative effects. The maximal power is then given by

$$\begin{aligned} P_{\max} &\approx \lambda\Psi^3\xi\sin\theta. \\ &\approx \frac{4\pi^4\rho h r^4 R_t H}{R_a T^3 R} \end{aligned} \tag{17}$$

Example: With the input parameters $T = 5s, \rho_{\text{metal}} = 8000kg/m^3, h = 0.3m$, $r = 0.5m$, $H = 0.5m$, $R = 3m$, $R_t = 0.725m$, $R_a = 0.020m$ we get

$$P_{\max} = 2840W. \tag{18}$$

4.1.2 Bifurcation and Stability Analysis

In the following we analyze the stability of the Dynamo under varying damping coming from the power production. We assume constant nutation angle and constant revolution speed of the driving motion corresponding to a perfect sinusoidal wave. With $x = \delta$ and $y = \delta'$ we

rewrite formula (27) from [Gulick and O'Reilly, 2000] to the first order system

$$\frac{d}{dt}x\left(t\right) = y\left(t\right)$$
$$\frac{d}{dt}y\left(t\right) = -ay\left(t\right) - b\cos\left(x\left(t\right)\right) + c\sin\left(x\left(t\right)\right) + d\sin\left(2\,x\left(t\right)\right) - a,$$

where $a = \frac{\zeta^2\nu}{1+\zeta^2\eta}, b = \frac{\zeta\,\eta\,\sin(\theta)}{1+\zeta^2\eta}, c = \frac{\zeta\,\nu\,\sin(\theta)}{1+\zeta^2\eta}, d = 1/2\,\frac{(\eta-1)(\sin(\theta))^2}{1+\zeta^2\eta}$. We are interested in varying the damping through the parameter $\nu = \frac{\sigma}{\lambda_2\Phi_0}$, where σ is the viscous damping.

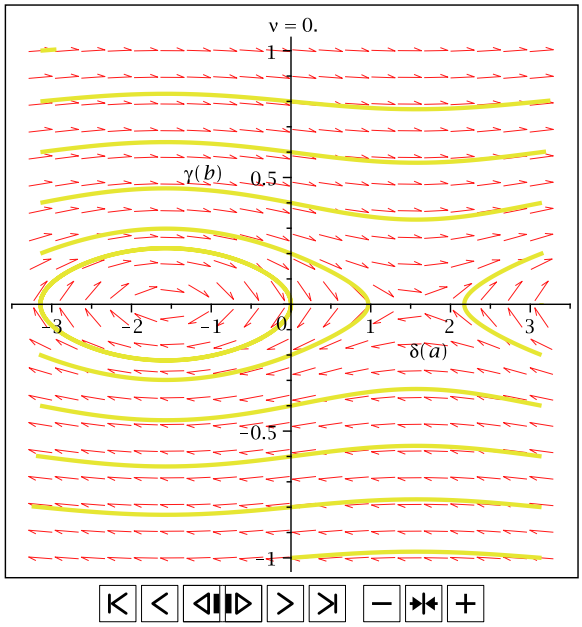

Figure 11: Phase portrait under varying viscous damping or power outtake. (To see the animation, please view the file in a suitable PDF viewer.)

An animation of the phase portrait under varying viscous damping or power outtake is shown on Figure 11. Starting with no damping we see periodic orbits oscillating around a stationary solution lying at $(-\pi/2, 0)$. This basin of periodic orbits is enclosed by the so-called separatrix consisting of the two orbits ending in the saddle point at $(+\pi/2, 0)$. Adding damping, the periodic orbits are attracted to the stationary solution but otherwise the overall picture is the same. For increased damping the two stationary solutions (the attracting point and the saddle point) moves further away from the origin until they meet approximately at $\pm\pi$. Any further damping causes the flywheel to stop. In this section we will determine this maximal damping, i.e., the maximal friction plus power production, and describe the systems dynamics in more detail as function of the damping.

In a stationary point $x' = y' = 0$ or

$$g(x, \sigma) = -b\cos(x) + c(\sigma)\sin(x) + d\sin(2x) - a(\sigma) = 0. \tag{19}$$

By the substitution $\cos(x) = \frac{1-t^2}{1+t^2}$, $\sin(x) = 2\,\frac{t}{1+t^2}$ and multiplication with $(1+t^2)^2$ we get

$$(b-a)\,t^4 + (-4\,d + 2\,c)\,t^3 - 2\,at^2 + (4\,d + 2\,c)\,t - b - a = 0. \tag{20}$$

One can solve this equation, and amongst the four (in general complex) roots only the real roots correspond to stationary points. Finally:

$$x = \arctan\left(\frac{2t}{1-t^2}\right). \tag{21}$$

When inserting the original physical parameters, the full formula (21) fills many pages. As further the numerical evaluation of this formula is up to 10^{-7} off, we advice to find the roots numerically or by one of the following approximate methods.

In [Gulick and O'Reilly, 2000] the values $a \approx 1 \cdot 10^{-2}$, $b \approx 2 \cdot 10^{-2}$, $c \approx 3 \cdot 10^{-4}$, $d \approx 1 \cdot 10^{-4}$ are used. And generally d is expected to be about two orders of magnitude smaller than a and b. Hence by setting $d = 0$ or $c = d = 0$ in Equation 19 simple and remarkably close estimates of the x-value of stationary points are found.

A bifurcation from two to no stationary points can only occur if

$$\frac{\partial}{\partial x} g(x, \sigma) = b\sin(x) + c(\sigma)\cos(x) + 2\,d\cos(2\,x) = 0 \tag{22}$$

The easiest way to find the critical damping is through a numerical implicit plot of Equation 19. An example is shown on Figure 12. Note that near maximal damping the stationary point moves very fast as a function of the damping. In fact $\|\frac{dx}{d\nu}\|$ of each stationary point tends to infinity which will cause problems later on.

4.1.3 Local Stability Around the Stationary Solutions

The local behavior close to the stationary points are determined by the Jacobian matrix

$$\begin{bmatrix} 0 & 1 \\ b\sin(x) + c\cos(x) + 2\,d\cos(2\,x) & -a \end{bmatrix} \tag{23}$$

with eigenvalues

$$-1/2\,a \pm 1/2\,\sqrt{a^2 + 4\,b\sin(x) + 16\,d\,(\cos(x))^2 + 4\,c\cos(x) - 8\,d}, \tag{24}$$

where $x = x(\sigma)$ is the x-coordinate of a stationary point and a and c both depend on the damping σ.

We immediately notice that when the two stationary points merge to one point Equation 22 implies that the lower left hand side term

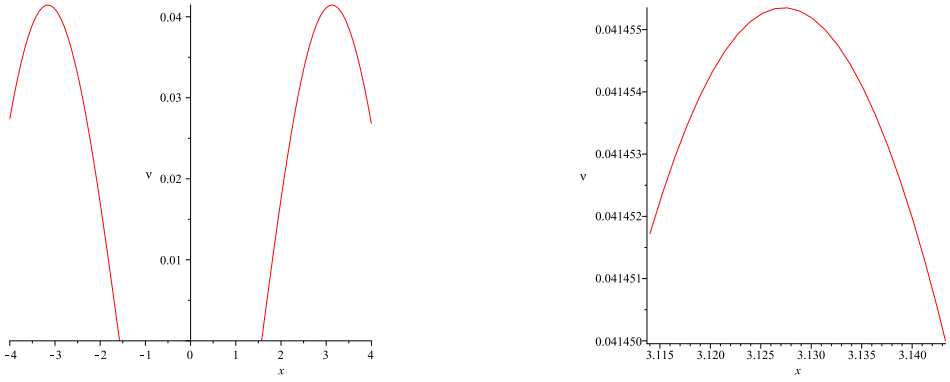

Figure 12: Left: A plot of the x-coordinate of the stationary points for varying damping through variation of the parameter ν. For each ν value the x-coordinates are given by the intersection between the shown graph and the horizontal ν constant line. The bifurcation where there the two stationary points coincides and disappears happens for $\nu \approx 0.0415$. Right: A zoom of near the bifurcation.

in the Jacobian is zero. Hence the to eigenvalues are 0 (zero) and $-a$ respectively and the one stationary point may be considered as a degenerate saddle point. By simply inserting the x-values of the two stationary points we see that:

- The "right hand side stationary point" starts as a saddle and ends as the degenerate saddle.
- The "left hand side stationary point" is the configuration the devise will end in under operating circumstances. It starts as a center, and by introducing damping it becomes an attracting spiral with a local attraction given by the real part of the eigenvalue $-a(\sigma)/2$. Hence the system stability is increased linearly with the damping σ. However for sufficiently large σ the term under the square root in the formula for the eigenvalues,

$$\begin{aligned} \text{discriminant} = \; & a^2(\sigma) + 4\,b\sin(x) + 16\,d\,(\cos(x))^2 && (25) \\ & + 4\,c(\sigma)\cos(x) - 8\,d && (26) \end{aligned}$$

  gets first zero then positive. In this σ-interval the two eigenvalues are both real numbers that go very fast from both being $-a/2$ to being $-a$ and 0 (zero). Hence, as $a(\sigma)$ and $c(\sigma)$ both increase linearly with σ but more important the x-value of the stationary point changes extremely fast with σ, the stationary point destabilizes extremely quickly in a very small σ-interval.
- Finally the two stationary points collides at $x \approx 3.13 < \pi$ with eigenvalues $-a$ and zero and for higher σ there are no stationary solutions and the flywheel stops.

We recommend to require that both

$\mathcal{A}$ the *discriminant* given by Equation 26 is negative under operating conditions and

$\mathcal{B}$ the maximal damping used is chosen such that the derivative $\|\frac{dx}{d\nu}\|$ of each stationary point still is small enough to allow practical control.

A final warning: Closely before the *discriminant* change from negative to become zero and positive we run into numerical problems when using standard function evaluation in Maple. That is, we can not follow the attractive stationary point closely enough to find a σ-value for which the *discriminant* is positive. Hence for practical purposes it seems that recommendation $\mathcal{B}$ implies $\mathcal{A}$.

4.2 Model 2

Next, we consider the slightly simpler model derived in [Ishii et al., 2011] which is illustrated in Fig. 13. The assumptions are similar to the ones for the model above, but θ is here a driving angle, with amplitude θ_0.

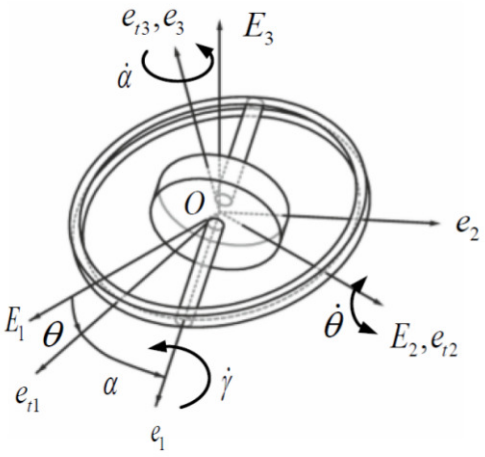

Figure 13: A simpel model of a gyroscopic device where the sinoidal rotation is along the diameter of the rotating plane (from [Ishii et al., 2011]).

4.2.1 Power Output

A maximal output power similar to the one for the model above has been derived in [Ishii et al., 2011]:

$$\begin{aligned} P_{\max} &\approx \lambda \Psi^3 \xi \theta_0 / 2. \\ &\approx \frac{2\pi^4 \rho h r^4 R_t \arcsin(H/R)}{R_a T^3} \end{aligned} \tag{27}$$

Using the same values for the input parameters as in the example we get:

$$P_{\max} = 1400W. \tag{28}$$

The order of magnitude for the power in this configuration is therefore 1 kW. We note that a wave with a waveheight of 1 meter has a power of about $2400W$ per meter width. Finally, comparing equations (18) and (28), we see that the estimated power output of this model is about half as large as the estimated power output of the other model.

4.2.2 Stability and Phase Portrait

We now numerically check the stability of the model by [Ishii et al., 2011] for the relevant design parameters of a $\sim 1\ kW$ generator.

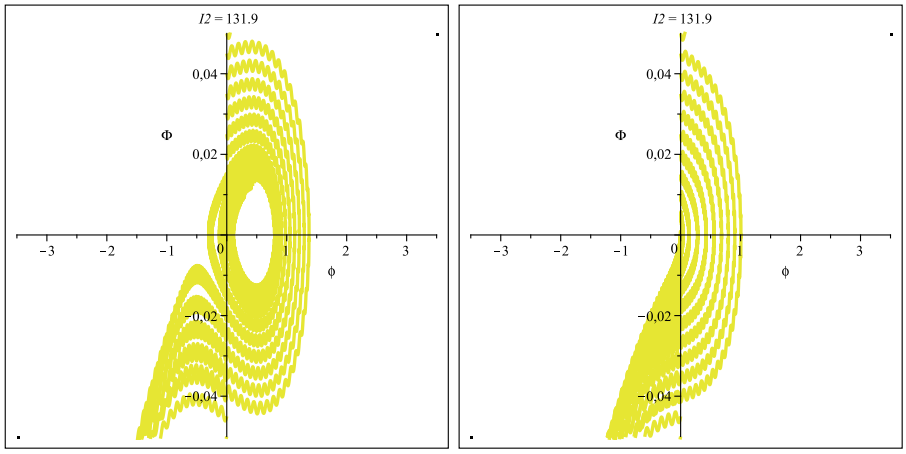

Figure 14: The phase-portrait of the model from Ishii et al. under sinusoidal driving. Left plot is for $\sigma = 0.9\sigma_{crit}$, for which there is a stable region around $\phi = 0.5$. Right plot is for $\sigma = 1.1\sigma_{crit}$ and the stability is lost in this case.

Assuming

$$\theta = \theta_0 \sin(\tau t)\,,\ \alpha = \phi + \tau t,$$

but *not* $\phi =$ constant, the upper Eq. (11) in [Ishii et al., 2011] turns into

$$\ddot{\phi}\left(\xi^2 I_1 + I_2\right) - \xi I_1 \theta_0 \tau^2 \sin(\tau t)\sin(\phi + \tau t) + \xi^2 \sigma\left(\dot{\phi} + \tau\right) + \left(I_2 - I_1\right)\theta_0^2 \tau^2 \cos^2(\tau t)\sin(\phi + \tau t)\cos(\phi + \tau t) = 0. \tag{29}$$

Introducing a new angle coordinate $\Phi = \dot{\phi}$, we have the non-linear

system of first order ODEs

$$\left[\begin{array}{c}\dot{\phi}\\ \dot{\Phi}\end{array}\right]=\left[\begin{array}{c}\Phi\\ \frac{1}{\xi^2 I_1+I_2}\xi I_1\theta_0\tau^2\sin(\tau t)\sin(\phi+\tau t)\end{array}\right]+$$
$$\left[\begin{array}{c}0\\ \frac{1}{\xi^2 I_1+I_2}\left[-(I_2-I_1)\theta_0^2\tau^2\cos^2(\tau t)\sin(\phi+\tau t)\cos(\phi+\tau t)-\xi^2\sigma\Phi-\xi^2\sigma\tau\right]\end{array}\right]. \tag{30}$$

Parameters to be used for the stability check for the prototype:

$$\zeta\equiv\xi=R_t/R_a=0.725/0.020=36.25, \tag{31a}$$
$$\lambda\equiv I_1=\frac{1}{2}mr^2=\frac{1}{2}\rho h\pi r^4=235.5, \tag{31b}$$
$$I_2=\frac{1}{12}m\left(3r^2+h^2\right)=\frac{1}{12}\rho h\pi r^2\left(3r^2+h^2\right)=131.9 \tag{31c}$$
$$\sigma_{\text{crit}}=\frac{I_1\theta_0\tau}{2\xi}=0.675 \tag{31d}$$
$$\tau=2\pi/T=1.257 \tag{31e}$$
$$\theta_0=\arcsin\left[\frac{H}{R}\right]=\arcsin\left[\frac{1/2}{3}\right]=0.1674 \tag{31f}$$

In Fig. 14 we plot some trajectories starting at the 'y-axis' to illustrate the stable region if $\sigma<\sigma_{crit}$. Hence the above numerical (Maple) exercise qualitativelly confirms the stability of the $\sim 1\ kW$ prototype. Further detailed investigations should be performed to understand the role of the different parameters (such as I_2). More general Fourier decomposed drivings could easilly be implemented to better model true water waves.

For the inventor it is also useful to know the rotational speed when chosing generator and ball bearings, and also the torque on the arm when chosing its dimensions. Using the following relations for the (stationary) power

$$P=\sigma\dot{\gamma}^2=\sigma\xi^2\dot{\alpha}^2=\sigma\xi^2\tau^2,$$

we can estimate the rotational speed of the flywheel. For example $P\sim 1400=0.675\cdot\dot{\gamma}^2=\sigma\xi^2\tau^2=0.675\cdot 36.25^2\cdot 1.257^2=1401$. hence the rotational speed is $\dot{\gamma}=\sqrt{1400/0.675}=45.54$ Hz. Taking this times 60 gives 2730 rpm. Using the estimate of Eq. (12) in [Heyda, 2002] translated to the notation of [Ishii et al., 2011] gives

$$T=\pm I_1\tau\dot{\gamma}.$$

With the parameters of the $\sim 1\ kW$ prototype we get a torque in the order of 13.5 kNm.

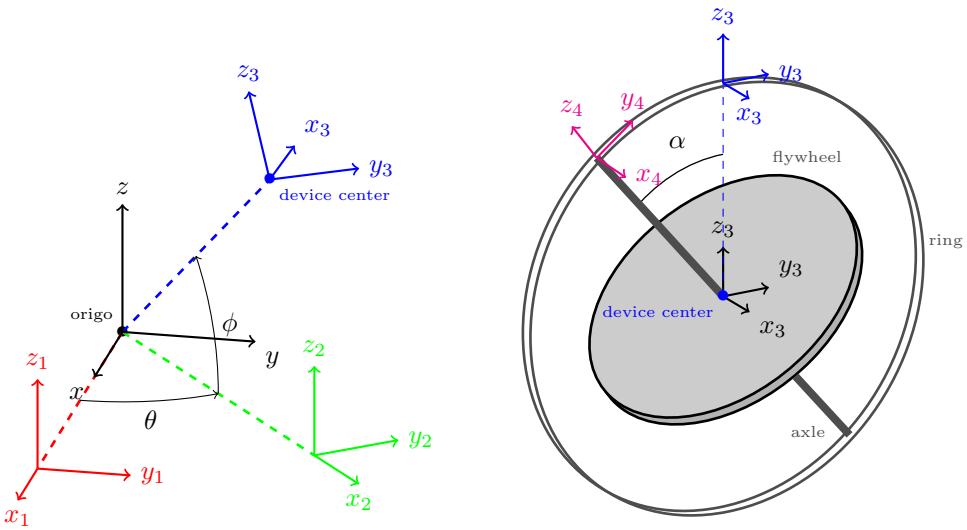

Figure 15: Sketch of the mechanical system and four coordinate systems. The origos of the coordinate frames have been translated to make the relations between these more obvious.

5 Model Derived from Analytical Mechanics

5.1 Generalised Coordinates and the Lagrangian

We consider the mechanical system depicted in figure 15. In an analytical mechanical approach to the model, we begin by noting that the flywheel is a mechanical system with a single degree of freedom (the rotation angle α around the x_3 axis as explained below) subject to time dependent constraints, the motion of the wave which accelerates the flywheel.

The time evolution of the system is thus a solution $\alpha = \alpha(t)$ to the the Euler-Lagrange equation

$$\frac{\mathrm{d}}{\mathrm{d}t}\frac{\partial \mathcal{L}}{\partial \dot{\alpha}} - \frac{\partial \mathcal{L}}{\partial \alpha} = 0, \tag{32}$$

which one can write down from the Lagrange function $\mathcal{L} = \mathcal{L}(\alpha, \dot{\alpha}, t)$.

The Lagrange function is the difference between the kinetic energy $T = T(\alpha, \dot{\alpha})$ and the potential energy $V = V(\alpha, \dot{\alpha})$. Since the gravitational potential energy is negligible, the Lagrangian function is just the rotational kinetic energy, T.

The rotational kinetic energy of a gyroscope, idealized as a uniform thin disc with massless axel, is equal to one half the value of the moment of inertia bilinear form contracted with the rotation vector ω.

$$\mathcal{L} = \frac{1}{2}\,\omega^T \mathbf{J} \omega \tag{33}$$

The moment of inertia tensor is diagonal in the (x_4, y_4, z_4)-coordinate frame. The aim of the following calculations is therefore to express the (total) rotation vector of the flywheel in this frame as well. We therefore need to relate the basic rotations of the arm and the housing to each other, through rotation matrices.

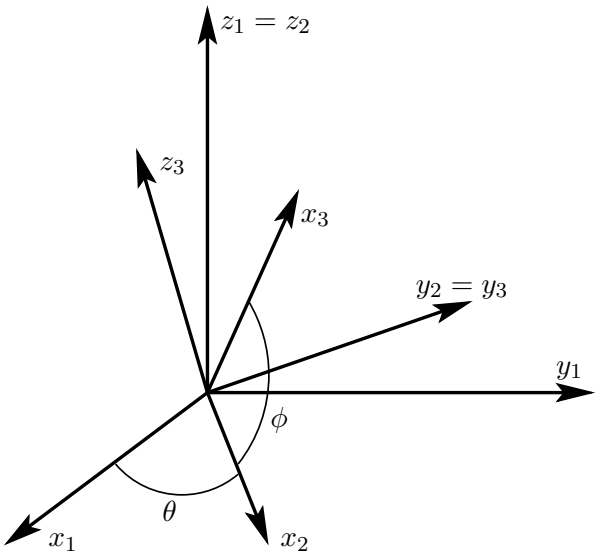

Figure 16: The three first coordinate systems.

To this end, we consider the four coordinate frames as sketched in figures 15 and repeated in figure 16. The (x_1, y_1, z_1) coordinate system is identical to the world coordinate system (x, y, z), such that the point of the arm (origo), to which the device is attached at the other end, is fixed in this frame. The (x_2, y_2, z_2) coordinate system is obtained by rotating around the z_1-axis with the angle θ. The (x_3, y_3, z_3) coordinate system is obtained by subsequently rotating around the y_2-axis with the angle ϕ. In this (x_3, y_3, z_3) coordinate system, the ring, in which the flywheel axle rolls, is fixed. Finally, the (x_4, y_4, z_4) coordinate system is obtained by subsequently rotating around the x_3-axis by the angle α. In this (x_4, y_4, z_4) coordinate system, the orientation of the flywheel axle is fixed, and the flywheel motion is simply a rotation around the z_4-axis.

Recall the basic rotation matrices, given by:

$$\mathbf{R}_x(\phi) = \begin{pmatrix} 1 & 0 & 0 \\ 0 & \cos\phi & -\sin\phi \\ 0 & \sin\phi & \cos\phi \end{pmatrix}, \tag{34}$$

$$\mathbf{R}_y(\phi) = \begin{pmatrix} \cos\phi & 0 & \sin\phi \\ 0 & 1 & 0 \\ -\sin\phi & 0 & \cos\phi \end{pmatrix}, \tag{35}$$

$$\mathbf{R}_z(\phi) = \begin{pmatrix} \cos\phi & -\sin\phi & 0 \\ \sin\phi & \cos\phi & 0 \\ 0 & 0 & 1 \end{pmatrix}. \tag{36}$$

The end of the arm (the point with coordinates $(x_2, y_2, z_2) = (R, 0, 0)$) has (x, y, z) coordinates

$$\mathbf{r} = \mathbf{R}_z(\theta)\mathbf{R}_y(\phi) \begin{pmatrix} R \\ 0 \\ 0 \end{pmatrix} = R \begin{pmatrix} \cos\theta\, \cos\phi \\ \sin\theta\, \cos\phi \\ -\sin\phi \end{pmatrix}. \tag{37}$$

The flywheel rotates around the z_4-axis so the rotation vector of the basic flywheel motion has (x_4, y_4, z_4) coordinates

$$\boldsymbol{\omega}_1 = \zeta\dot{\alpha} \begin{pmatrix} 0 \\ 0 \\ 1 \end{pmatrix}, \tag{38}$$

where ζ is the ratio between the radii. The coordinates of the rotation vector of the α rotation has the same coordinates with respect to both (x_2, y_2, z_2) and (x_3, y_3, z_3) system namely

$$\boldsymbol{\omega}_2 = \dot{\alpha} \begin{pmatrix} 1 \\ 0 \\ 0 \end{pmatrix}. \tag{39}$$

The ϕ rotation is about the y_2-axis which is the same as the y_3-axis, so the rotation vector has (x_4, y_4, z_4) coordinates

$$\boldsymbol{\omega}_3 = \dot{\phi}\, \mathbf{R}_x(\alpha)^T \begin{pmatrix} 0 \\ 1 \\ 0 \end{pmatrix} = \dot{\phi} \begin{pmatrix} 0 \\ \sin\alpha \\ \cos\alpha \end{pmatrix}. \tag{40}$$

Finally we have the θ rotation around the z-axis which is the same as the z_1-axis, so the rotation vector has (x_4, y_4, z_4) coordinates

$$\boldsymbol{\omega}_4 = \dot{\theta}\, \mathbf{R}_x(\alpha)^T \mathbf{R}_y(\phi)^T \begin{pmatrix} 0 \\ 0 \\ 1 \end{pmatrix} = \dot{\theta} \begin{pmatrix} \sin\phi \\ \cos\phi\, \sin\alpha \\ \cos\phi\, \cos\alpha \end{pmatrix}. \tag{41}$$

The total rotation vector has (x_4, y_4, z_4) coordinates

$$\boldsymbol{\omega} = \boldsymbol{\omega}_1 + \boldsymbol{\omega}_2 + \boldsymbol{\omega}_3 + \boldsymbol{\omega}_4. \tag{42}$$

The moments of inertia of the flywheel in (x_4, y_4, z_4) coordinates are

$$\mathbf{J} = \begin{pmatrix} J_2 & 0 & 0 \\ 0 & J_2 & 0 \\ 0 & 0 & J_1 \end{pmatrix}, \tag{43}$$

where

$$J_1 = \frac{1}{2}\, m\, r^2, \qquad J_2 = \frac{1}{12}\, m\, (3r^2 + h^2). \tag{44}$$

Observe that if $h \ll r$ the we have $J_2 \approx J_1/2$. The rotational energy is

$$E_r = \frac{1}{2}\, \boldsymbol{\omega}^T\, \mathbf{J}\, \boldsymbol{\omega}. \tag{45}$$

If apply the approximation $J_2 \approx J_1/2$ then we obtain

$$\begin{aligned} \frac{E_r}{J_1} = \frac{1+2\zeta^2}{4}\, \dot\alpha^2 + \left(\frac{1}{2}\dot\theta\, \sin\phi + \zeta\, \cos\alpha\, (\dot\theta \cos\phi + \dot\phi)\right) \dot\alpha \\ + \frac{1}{4} \cos^2\alpha\, (\dot\theta\cos\phi + \dot\phi)^2 + \frac{1}{4}\left(\dot\phi^2 + \dot\theta^2 + 2\dot\phi\,\dot\theta\, \cos\phi\right). \end{aligned} \tag{46}$$

We assume that the center of mass is at the end of the arm, i.e., at the point $\mathbf{r}$, see (37). The translational kinetic energy is then

$$E_t = \frac{1}{2} m \|\dot{\mathbf{r}}\|^2 = \frac{1}{2} m (\dot\theta^2 \cos^2\phi + \dot\phi^2). \tag{47}$$

The Lagrangian of the system is then (up to a factor $\frac{1}{2}m$) given by

$$\begin{aligned} \mathcal{L} = \dot\theta^2 \cos^2\phi + \dot\phi^2 \\ + r^2 \left(\frac{1+2\zeta^2}{4}\, \dot\alpha^2 + \left(\frac{1}{2}\dot\theta\, \sin\phi + \zeta\, \cos\alpha\, (\dot\theta \cos\phi + \dot\phi)\right)\, \dot\alpha \right. \\ \left. + \frac{1}{4} \cos^2\alpha\, (\dot\theta\cos\phi + \dot\phi)^2 + \frac{1}{4}\left(\dot\phi^2 + \dot\theta^2 + 2\dot\phi\,\dot\theta\, \cos\phi\right)\right). \end{aligned} \tag{48}$$

5.2 Prescribed Motion

We are given now a forcing of the center of mass (i.e., we ignore the fluid interaction and just assume that the system follows the movement of the water). Then θ and ϕ are given and the only dynamical variable is α. Observe, that the first two and the last term in (48) are independent of α, so we can ignore them, as they will not enter the equations of motion. The Lagrangian of the system is then (up to new factor of r^2) given by

$$\begin{aligned} \mathcal{L} = \frac{1+2\zeta^2}{4} \left(\frac{\mathrm{d}\alpha}{\mathrm{d}t}\right)^2 + \left(\frac{1}{2}\dot\theta\, \sin\phi + \zeta\, \cos\alpha\, (\dot\theta \cos\phi + \dot\phi)\right) \frac{\mathrm{d}\alpha}{\mathrm{d}t} \\ + \frac{1}{4} \cos^2\alpha\, (\dot\theta\cos\phi + \dot\phi)^2. \end{aligned} \tag{49}$$

We have

$$\begin{pmatrix} \cos\theta\,\cos\phi \\ \sin\theta\,\cos\phi \\ -\sin\phi \end{pmatrix} = \begin{pmatrix} x(t) \\ y(t) \\ z(t) \end{pmatrix}, \quad \text{with} \quad x(t)^2 + y(t)^2 + z(t)^2 = 1. \tag{50}$$

Differentiation with respect to t yields

$$-\dot{\phi} \begin{pmatrix} \cos\theta\,\sin\phi \\ \sin\theta\,\sin\phi \\ \cos\phi \end{pmatrix} + \dot{\theta} \begin{pmatrix} -\sin\theta\,\cos\phi \\ \cos\theta\,\cos\phi \\ 0 \end{pmatrix} = \begin{pmatrix} x'(t) \\ y'(t) \\ z'(t) \end{pmatrix}. \tag{51}$$

These equations are easily solved to give

$$\sin\phi = -z(t) \qquad \cos\phi = \sqrt{1 - z(t)^2}, \tag{52}$$

$$\sin\theta = \frac{y(t)}{\sqrt{1 - z(t)^2}}, \quad \cos\theta = \frac{x(t)}{\sqrt{1 - z(t)^2}}, \tag{53}$$

$$\dot{\phi} = \frac{z'(t)}{\sqrt{1 - z(t)^2}}, \qquad \dot{\theta} = \frac{(1 - z(t)^2)y'(t) - y(t)\,z(t)\,z'(t)}{x(t)(1 - z(t)^2)}. \tag{54}$$

This are now substituted into (49) and we are ready to write down the equation of motions

$$\frac{\mathrm{d}}{\mathrm{d}t}\frac{\partial \mathcal{L}}{\partial \dot{\alpha}} - \frac{\partial \mathcal{L}}{\partial \alpha} = F(\alpha, \dot{\alpha}, \mathbf{r}(t)), \tag{55}$$

where F represents the force from the power generator inside the housing. It could also contain other losses in the system. For the initial analysis we assume that the only contribution to F is from the power generator and we want to design the control F such that the total energy gain

$$\mathcal{E} = \int_0^T F\,\mathrm{d}t \tag{56}$$

is maximised.

5.3 Prescribed Forces

What have to be changed if we have prescribed forces on the system instead of a prescribed motion? First of all, θ, ϕ will then become variables in the system so in the end we will have three coupled second order equations.

The rigid "arm" absorbs some of the force and the remaining effective outer force must lie in the $y_2 z_2$-plane. We need to transform this force into a generalised force in the $\theta\phi$-plane.

Given a force $\mathbf{F}$ with $\mathbf{r} \cdot \mathbf{F} = 0$ (obtained by projection into the plane orthogonal to $\mathbf{r}$), then the generalised forces Θ, Φ are give by the same equations as (51). That is,

$$-\Phi \begin{pmatrix} \cos\theta\,\sin\phi \\ \sin\theta\,\sin\phi \\ \cos\phi \end{pmatrix} + \Theta \begin{pmatrix} -\sin\theta\,\cos\phi \\ \cos\theta\,\cos\phi \\ 0 \end{pmatrix} = \mathbf{F} = \begin{pmatrix} F_1 \\ F_2 \\ F_3 \end{pmatrix}. \tag{57}$$

Thus

$$\Phi = \frac{-F_3}{\cos\phi}, \qquad \Theta = \frac{F_2\,\cos\phi - F_3\,\sin\theta\,\sin\phi}{\cos\theta\,\cos^2\phi}. \tag{58}$$

We can no longer ignore the terms we removed to obtain (49). Instead we have to use (48). We have

$$\frac{\partial\mathcal{L}}{\partial\dot\alpha} = r^2\left(\frac{1+2\zeta^2}{2}\dot\alpha + \frac{1}{2}\,\dot\theta\,\sin\phi + \zeta\,\cos\alpha\,(\dot\theta\cos\phi + \dot\phi)\right), \tag{59}$$

$$\frac{\partial\mathcal{L}}{\partial\alpha} = r^2\left(-\zeta\,\sin\alpha\,(\dot\theta\cos\phi + \dot\phi)\,\dot\alpha - \frac{1}{2}\cos\alpha\,\sin\alpha\,(\dot\theta\cos\phi + \dot\phi)^2\right), \tag{60}$$

$$\frac{\partial\mathcal{L}}{\partial\dot\theta} = 2\,\dot\theta\,\cos^2\theta + r^2\left(\frac{1}{2}\dot\theta + \frac{1}{2}\dot\phi\,\cos\phi + \left(\frac{1}{2}\sin\phi + \zeta\,\cos\alpha\,\cos\phi\right)\dot\alpha + \frac{1}{2}\cos^2\alpha\,\cos\phi(\dot\theta\,\cos\phi + \dot\phi)\right), \tag{61}$$

$$\frac{\partial\mathcal{L}}{\partial\theta} = -2\,\dot\theta^2\cos\theta\,\sin\theta, \tag{62}$$

$$\frac{\partial\mathcal{L}}{\partial\dot\phi} = 2\,\dot\phi + r^2\left(\frac{1}{2}\dot\phi + \frac{1}{2}\dot\theta\,\cos\phi + \zeta\,\dot\alpha\,\cos\alpha + \frac{1}{2}\cos^2\alpha\,(\dot\theta\,\cos\phi + \dot\phi)\right), \tag{63}$$

$$\frac{\partial\mathcal{L}}{\partial\phi} = r^2\left(\left(\frac{1}{2}\dot\theta\,\cos\phi - \zeta\,\dot\theta\,\cos\alpha\,\sin\phi\right)\dot\alpha - \frac{1}{2}\dot\theta\,\cos^2\alpha\,\sin\phi(\dot\theta\,\cos\phi + \dot\phi) - \frac{1}{2}\dot\phi\,\dot\theta\,\sin\phi\right). \tag{64}$$

The Euler Lagrange equations read

$$\frac{\mathrm{d}}{\mathrm{d}t}\,\frac{\partial\mathcal{L}}{\partial\dot\alpha} - \frac{\partial\mathcal{L}}{\partial\alpha} = F(\alpha,\dot\alpha,\mathbf{r}(t)), \tag{65}$$

$$\frac{\mathrm{d}}{\mathrm{d}t}\,\frac{\partial\mathcal{L}}{\partial\dot\theta} - \frac{\partial\mathcal{L}}{\partial\theta} = \Theta, \tag{66}$$

$$\frac{\mathrm{d}}{\mathrm{d}t}\,\frac{\partial\mathcal{L}}{\partial\dot\phi} - \frac{\partial\mathcal{L}}{\partial\phi} = \Phi. \tag{67}$$

That is,

$$r^2\Big(\frac{1+2\zeta^2}{2}\ddot\alpha + \frac{1}{2}\,\ddot\theta\,\sin\phi + \frac{1}{2}\,\dot\theta\,\dot\phi\,\cos\phi - \zeta\,\dot\alpha\,\sin\alpha\,(\dot\theta\cos\phi + \dot\phi) + \zeta\,\cos\alpha\,(\ddot\theta\cos\phi - \dot\theta\,\dot\phi\sin\phi + \ddot\phi) + \zeta\,\sin\alpha\,(\dot\theta\cos\phi + \dot\phi)\,\dot\alpha + \frac{1}{2}\cos\alpha\,\sin\alpha\,(\dot\theta\cos\phi + \dot\phi)^2\Big) = F(\alpha,\dot\alpha,\mathbf{r}(t)), \tag{68}$$

$$2\,\ddot{\theta}\,\cos^2\theta - 4\dot{\theta}^2\,\cos\theta\,\sin\theta + 2\,\dot{\theta}^2\cos\theta\,\sin\theta + r^2\left(\frac{1}{2}\ddot{\theta} + \frac{1}{2}\ddot{\phi}\cos\phi - \frac{1}{2}\dot{\phi}^2\sin\phi\right.$$
$$+\left(\frac{1}{2}\,\sin\phi + \zeta\,\cos\alpha\,\cos\phi\right)\,\ddot{\alpha} + \left(\frac{1}{2}\dot{\phi}\cos\phi - \zeta\,\dot{\alpha}\sin\alpha\,\cos\phi - \zeta\,\dot{\phi}\cos\alpha\,\sin\phi\right)\,\dot{\alpha}$$
$$-\cos\alpha\,\sin\alpha\,\cos\phi\,(\dot{\theta}\,\cos\phi + \dot{\phi})\dot{\alpha} - \frac{1}{2}\cos^2\alpha\,\sin\phi\,(\dot{\theta}\,\cos\phi + \dot{\phi})\dot{\phi}$$
$$\left.+\frac{1}{2}\cos^2\alpha\,\cos\phi\,(\ddot{\theta}\,\cos\phi - \dot{\theta}\,\dot{\phi}\,\sin\phi + \ddot{\phi})\right) = \frac{F_2\,\cos\phi - F_3\sin\theta\,\sin\phi}{\cos\theta\,\cos^2\phi}, \tag{69}$$

$$2\ddot{\phi} + r^2\left(\frac{1}{2}\ddot{\phi} + \frac{1}{2}\ddot{\theta}\,\cos\phi - \frac{1}{2}\dot{\theta}\,\dot{\phi}\,\sin\phi + \zeta\ddot{\alpha}\,\cos\alpha - \zeta\dot{\alpha}^2\,\sin\alpha\right.$$
$$-\cos\alpha\,\sin\alpha\,(\dot{\theta}\,\cos\phi + \dot{\phi})\,\dot{\alpha} + \frac{1}{2}\cos^2\alpha\,(\ddot{\theta}\,\cos\phi - \dot{\theta}\,\dot{\phi}\,\sin\phi + \ddot{\phi})$$
$$-\left(\frac{1}{2}\dot{\theta}\,\cos\phi - \zeta\,\dot{\theta}\,\cos\alpha\,\sin\phi\right)\dot{\alpha} + \frac{1}{2}\dot{\theta}\,\cos^2\alpha\,\sin\phi(\dot{\theta}\,\cos\phi + \dot{\phi})$$
$$\left.+\frac{1}{2}\dot{\phi}\,\dot{\theta}\,\sin\phi\right) = \frac{-F_3}{\cos\phi}. \tag{70}$$

This set of equations will determine the motion of the flywheel and the supporting arm.

6 Conclusions

This project report has analysed a gyroscopic device for conversion of mechanical energy in ocean surface waves to electrical energy.

We have firstly estimated, from standard engineering mechanics, expressions for the power production of the device, due to both a planar motion model, and a conic motion model.

Secondly, we have established a simple analytical model, based on analytical mechanics, which permits a study of the power production as a function of system parameters and any motion of the device.

In general, we find that it is possible to extract a significant amount of energy from an ocean wave using the described device. Our models open up for a design optimization.

Studies of the actual motion of the device when subjected to waves at sea, of the initiation procedure of the device, of transient effects in operating conditions, and of threshold motion for the operation of the device are still lacking.

References

Rameswar Bhattacharyya. *Dynamics of Marine Vehicles (Ocean engineering)*. John Wiley & Sons Inc, 1978. ISBN 0471072060.

J. Falnes. *Ocean Waves and Oscillating Systems: Linear Interactions Including Wave-Energy Extraction*. Cambridge University Press, 1 edition, 2002. ISBN 0521782112.

P. R. Fish, R. B. Dean, and N. J. Heaf. Fluid-structure interaction in morison's equation for the design of offshore structures. *Engineering Structures*, 2(1):15 – 26, 1980. ISSN 0141-0296. doi: DOI:10.1016/0141-0296(80)90025-5.

A. Gams, L. Zlajpah, and J. Lenarcic. Imitating human acceleration of a gyroscopic device. *Robotica*, 25:501 – 509, 2007.

C.J. Garrison. Water impact loads on circular structural members. *Applied Ocean Research*, 18(1):45–54, 1996.

D. W. Gulick and O. M. O'Reilly. On the dynamics of the dynabee. *Journal of Applied Mechanics*, 67(2):321–325, 2000.

P. G. Heyda. Roller ball dynamics revisited. *American Journal of Physics*, 70(10):1049–1051, 2002. ISSN 00029505. doi: DOI: 10.1119/1.1499508.

L.H. Holthuijsen. *Waves in oceanic and coastal waters*. Cambridge University Press, 2007. ISBN 9780521860284.

T. Ishii, J. Iwasaki, and H. Hosaka. Study on dynamic characteristics of gyroscopic power generator. *International Journal of Applied Electromagnetics and Mechanics*, 36:131–139, 2011. doi: 10.3233/JAE-2011-1351.

A.L. Mischler, 1973. 'Gyroscopic device,' U.S. Patent 3726146.

Kunihiro Ogihara. Theoretical analysis on the transverse motion of a buoy by surface wave. *Applied Ocean Research*, 2(2):51 – 56, 1980. ISSN 0141-1187. doi: DOI:10.1016/0141-1187(80)90029-2.

J. Olsen, 2011a. Personal communication.

J. Olsen, 2011b. PA 2011 00073, Patent Application in Progress.

P.A. Smith and P.K. Stansby. Viscous oscillatory flows around cylindrical bodies at low keulegan-carpenter numbers using the vortex method. *Journal of Fluids and Structures*, 5(4):339–361, 1991.